

Journal of Materials Chemistry A

Accepted Manuscript



This is an *Accepted Manuscript*, which has been through the Royal Society of Chemistry peer review process and has been accepted for publication.

Accepted Manuscripts are published online shortly after acceptance, before technical editing, formatting and proof reading. Using this free service, authors can make their results available to the community, in citable form, before we publish the edited article. We will replace this *Accepted Manuscript* with the edited and formatted *Advance Article* as soon as it is available.

You can find more information about *Accepted Manuscripts* in the [Information for Authors](#).

Please note that technical editing may introduce minor changes to the text and/or graphics, which may alter content. The journal's standard [Terms & Conditions](#) and the [Ethical guidelines](#) still apply. In no event shall the Royal Society of Chemistry be held responsible for any errors or omissions in this *Accepted Manuscript* or any consequences arising from the use of any information it contains.

Synthesis and performance studies of Zr-doped and W-Zr-codoped VO₂ nanoparticles and derived flexible foils

*Nan Shen,¹ Shi Chen,¹ Zhang Chen,¹ Xinling Liu,¹ Chuanxiang Cao,¹
Bingrong Dong,¹ Hongjie Luo,^{1,2} Jianjun Liu,¹ and Yanfeng Gao^{1,2*}*

¹Shanghai Institute of Ceramics (SIC), Chinese Academy of Sciences (CAS), Dingxi
1295, Changning, Shanghai, 200050, China

²School of Materials Science and Engineering, Shanghai University, Shangda Rd. 99,
Baoshan, Shanghai 200444, China

* Author for correspondence. Yanfeng Gao, Shanghai University,
Email: yfgao@shu.edu.cn, Tel/Fax: +86-21-6990-6218

Abstract

Vanadium dioxide (VO_2) is a key material for thermochromic smart window application because of its Mott phase transition properties. However, the application of VO_2 has been restricted for its drawbacks in performance, including high phase transition temperature (T_c), low luminous transmittance (T_{lum}), limited solar energy modulation ability (ΔT_{sol}) and unpleasant color. Various works have been doing to solve these problems, but the improvement in one aspect is always accompanied by the deterioration of the others. This paper reports that Zr doping can simultaneously decrease T_c , increase T_{lum} , improve ΔT_{sol} and modify the color of the VO_2 foils. The T_c decreased from 68.6 °C to 64.3 °C at 9.8 % Zr-doping, and meanwhile, the composite foils prepared from Zr-doped VO_2 nanoparticles exhibited excellent luminous transmittance (up to 60.4 %) and solar energy modulation ability (up to 14.1 %). The experimental optical band gap was 1.59 eV for the undoped VO_2 , which was increased to 1.89 eV at 9.8 % doping. As a result, the color of the Zr-doped foils was modified to increase their luminous transmittance and lighten the yellowish color of the VO_2 foil. A first principle calculation was in good agreement with the experiment results. The W-Zr-codoped VO_2 nanoparticles were prepared to further decrease the transition temperature (28.6 °C) and meanwhile maintain the luminous transmittance (48.6 %) and solar energy modulation ability (4.9 %) of the derived foils.

Keywords: vanadium dioxide; phase transition temperature; luminous transmittance; solar energy modulation ability; band gap; color; doping

Introduction

Vanadium dioxide (VO_2) is a well-known inorganic thermochromic material,¹⁻³ which exhibits a reversible first-order metal-semiconductor transition (MST) at a critical temperature (T_c) of approximately 68 °C. The MST is accompanied by a structural change from a low temperature monoclinic phase ($P2_1/c$, M1) of an infrared-transparent semiconductor state to a high-temperature rutile phase ($P4_2/mnm$, R) of an infrared-reflective metallic state while maintaining the luminous transmittance. This distinct characteristic of VO_2 makes it more promising in the application to smart windows,⁴⁻⁸ compared with other inorganic and polymeric thermochromic materials.

However, some of shortcomings of VO_2 in properties such as high phase transition temperature, low luminous transmittance (T_{lum}) and limited solar energy modulation ability (ΔT_{sol}) become obstacles to its practical applications. Except that the temperature (T_c) of bulk VO_2 (68 °C) should be lowered to approach room temperature (20 °C⁹), the T_{lum} should exceed 40% to meet the needs of daytime lighting,¹⁰ and the ΔT_{sol} should be high enough for better energy-saving (more than 10%¹⁰). Besides, the unfavorable yellowish color of VO_2 films should be modified from the perspective of aesthetic.

Various attempts have been made to overcome these shortcomings. In order to reduce the T_c , the current strategies mainly involve elemental doping (decrease of 23 °C /at. % W^{6+} and 15 °C /at. % Mo^{6+})¹¹⁻¹⁴, and controlling of stress¹⁵, size effect¹⁶, non-stoichiometry¹⁷. To enhance the T_{lum} and ΔT_{sol} , designing multi-layer structured films (TiO_2/VO_2 ^{8,18}, $\text{TiO}_2/\text{VO}_2/\text{TiO}_2$ ¹⁹, and $\text{TiO}_2/\text{VO}_2/\text{TiO}_2/\text{VO}_2/\text{TiO}_2$ ²⁰), synthesizing composite foils²¹ and nanoporous films^{22,23}, and doping (Mg^{2+} , Ti^{4+})²⁴⁻²⁶ have been confirmed effective. Besides, doping with Mg^{2+} ²⁵ and F^{-} ²⁷ turns out to be beneficial to lighten the yellowish color of the VO_2 foils. However, none of these solutions can solve all problems in the properties of VO_2 . Therefore, a novel or a combination of these existing solutions is urgently needed to simultaneously regulate T_c , T_{lum} , ΔT_{sol} and color for the application to smart windows.

Doping has been proved to be an effective strategy to regulate the properties of VO₂, and doping with different metal ions could make differences on the T_c , T_{lum} , ΔT_{sol} or the color. Our previous work has shown that F doping can not only decrease T_c (from 66 °C at 0.0 at. % doping to 35 °C at 2.93 at. % doping) but also increase the T_{lum} and lighten the yellowish color of the VO₂ foil.²⁷ The following study of Mg-doped VO₂ composite foils finds that Mg doping decreases the T_c by 2 °C per at. %, and also causes a blue-shift in the absorption edge from 490 nm (2.53 eV) to 440 nm (2.82 eV) at 3.8 at. % Mg doping which results in the improved T_{lum} (from 45.3 % to 54.2 %) and the yellowness fading.²⁵ Similar results have been found in other researches.^{24,28} A recent work of Ti-doped VO₂ composite foils confirms that 1.1 at. % Ti doping achieves the simultaneous improvement of T_{lum} and ΔT_{sol} .²⁶ However, doping of the above elements can only solve part of problems, and simultaneous modulation of T_c , T_{lum} , ΔT_{sol} and color of VO₂ remains a problem.

The electronegativity (1.33) of zirconium is lower than vanadium (1.63), and could serve as ‘donors’ in VO₂. The ionic radius (Zr⁴⁺, 72 pm) is larger than V⁴⁺ (58 pm), which may lead to the instability of monoclinic VO₂, and is beneficial to T_c reduction.²⁹ Moreover, the wide band gap of ZrO₂ is beneficial to widen the bandgap between V_{3d} and O_{2p} states, thus can increase the luminous transmittance.^{27,30} Current studies of VO₂-based V-Zr-O films mainly focus on multi-layer structured and composite VO₂ films.³⁰⁻³¹ Xu *et al.*³¹ found that using ZrO₂ as an anti-reflecting layer greatly enhanced the luminous transmittance of VO₂ (from 32.3 % to 50.5 %). Our previous study of VO₂-ZrV₂O₇ composite film³⁰ showed a significant enhancement in T_{lum} (from 32.3 % at Zr/V =0 to 53.4 % at Zr/V=0.12) due to absorption-edge changes in the composites. No study to date has been done on Zr-doping behaviours in VO₂ nanoparticles and VO₂ foils³²⁻³⁴.

Based on these considerations, we used a hydrothermal method to prepare Zr-doped VO₂ nanoparticles, which were then used as the building blocks to construct VO₂ polymer composite foils. Through careful characterizations, Zr dopant was successfully demonstrated in the VO₂ nanoparticles. The Zr dopant can decrease the T_c , improve the T_{lum} and ΔT_{sol} as well as modify the color of VO₂ foils simultaneously.

However, T_c could be reduced only to 64.3 °C at the Zr doping amount of 9.8 %, although T_{lum} , ΔT_{sol} and yellowish color were simultaneously improved. Many previous studies have shown that W element is one of the most effective dopants upon the reduction of T_c due to introduced distortion and injected charges in VO_2 ,^{11,12} thus the W-Zr-codoped VO_2 nanoparticles were prepared to further decrease the transition temperature (28.6 °C) and meanwhile to maintain the luminous transmittance (48.6 %) and solar energy modulation ability (4.9 %) of the derived foils.

Experimental and Theoretical Methods

Preparation of Zr-doped and W-Zr-codoped VO_2 nanoparticles and derived VO_2 -PU composite foils. All reagents were of analytical grade and were used without further purification. In a typical hydrothermal synthesis, 0.125 g V_2O_5 powder and the requisite quantity of $\text{ZrOCl}_2 \cdot 8\text{H}_2\text{O}$ dopant were added into 40 mL of 0.15 M aqueous $\text{H}_2\text{C}_2\text{O}_4 \cdot 2\text{H}_2\text{O}$ to form a yellowish slurry. The slurry was stirred for 10 min and transferred to a 50 mL Teflon-lined stainless-steel autoclave. The autoclave was maintained at 260 °C for 24 h and then air-cooled to room temperature. The final product was collected via centrifugation, washed three times with deionized water and dried in a vacuum oven at 60 °C for 12 h. W-Zr-codoped VO_2 nanoparticles were prepared in the same process and ammonium tungstate ($(\text{NH}_4)_{10}\text{H}_2(\text{W}_2\text{O}_7)_6$) was used as W doping agent and added directly to the prepared yellowish slurry. The VO_2 -polyurethane (PU) thermochromic composite foils were prepared according to the following step.^{32,33} The as-prepared doped VO_2 nanoparticles were dispersed in deionised water with continuous stirring for 10 min and an appropriate quantity (one fiftieth of water amount, in volume) of the silane coupling agent KH-570 was added with ultrasonic treatment for approximately 30 min. Then, PU ($(\text{C}_{10}\text{H}_8\text{N}_2\text{O}_2 \cdot \text{C}_6\text{H}_{14}\text{O}_3)_n$, DISPERCOLL U54, Bayer) was added gradually with stirring over 10 min. Finally, the suspension was uniformly cast onto a polyethylene terephthalate (PET) substrate using an automatic coating machine and dried at 80 °C for 1 min.

Characterization. The morphologies and element compositions of the resulting powders were analysed via transmission electron microscopy (TEM, JEM2010, JEOL, Japan) with an energy-dispersive spectrometer (EDS) attachment. The crystalline structures of the resultant products were characterized with a Rigaku D/max 2550V X-ray diffractometer (Japan) with Cu K α radiation ($\lambda = 0.15406$ nm). The final doping ratios were determined by inductively coupled plasma measurement (ICP, Thermoelectric Corporation, IRIS Intrepid). X-ray photoelectron spectrometry (XPS) was performed with an Axis ultra DLD instrument using monochromatic Al K α radiation after 1 keV argon-ion etching for 10 s. The phase transition temperatures of the products were measured via differential scanning calorimetry (DSC, DSC200F3, NETZSCH) in nitrogen flow in the temperature range from 0 °C to 100 °C at a heating rate of 10 °C min⁻¹. The spectrum characteristics of the VO₂-PU composite foils were monitored in the range of 240-2600 nm on a Hitachi U-4100 UV visible-near-IR spectrophotometer equipped with a film heating unit. For all samples, the integral luminous transmittance (T_{lum} , 380-780 nm) and solar transmittance (T_{sol} , 240-2600 nm) were obtained based on the measured spectra using the following equation:

$$T_i = \int \varphi_i(\lambda)T(\lambda)d\lambda / \int \varphi_i(\lambda)d\lambda \quad (1)$$

$$\Delta T_{sol} = T_{sol}(T < T_c) - T_{sol}(T > T_c) \quad (2)$$

where $T(\lambda)$ denotes the transmittance at wavelength λ , i denotes ‘lum’, or ‘sol’ for the calculations, T and ΔT_{sol} are the temperature and solar energy modulation ability, φ_{lum} is the standard luminous efficiency function for the photopic vision, and φ_{sol} are the solar irradiance spectrum for the air mass 1.5 (corresponding to the sun standing 37° above the horizon). The color of the VO₂ foils was evaluated using a Konica Minolta CM2600d spectrophotometer.

Ab initio calculations. Periodic DFT calculations were performed using the VASP code.³⁵ The exchange and correlation items were described using a generalized gradient approximation (PBE-GGA).³⁶ To improve the treatment of electronic correlations in our DFT calculations, the Hubbard on-site repulsion U was taken into

account within the so-called GGA+U approximation.³⁷ The effective strength of the interaction (U_{eff} , $U_{\text{eff}} = U - J$) was set at 4.6 eV, in which U (5.3 eV) is the on-site Hubbard repulsion and J (0.7 eV) is Hund's exchange interaction.³⁸ The electron-ion interactions were described using the projector augmented wave (PAW) method, and valence electrons were treated explicitly with a plane-wave basis set at a cut-off energy of 400 eV.

Results and discussion

The as-synthesized Zr-doped VO₂ (M1) nanoparticles

The X-ray diffraction (XRD) patterns of the synthesized VO₂ nanoparticles with various Zr concentrations were shown in Figure 1a. All the peaks matched well with standard JCPDS No.72-0514 ($a=0.574$ nm, $b=0.452$ nm, $c=0.538$ nm, and $\beta=122.61^\circ$), indexing to monoclinic VO₂ (M1) phase with the space group P2₁/c (14). No other phases were observed, suggesting the formation of pure VO₂ (M1) structure. Since the radius of Zr⁴⁺ (72 pm) was slightly larger than that of V⁴⁺ (58 pm), a tiny migration of the (200) peak to small angles were detected (Figure 1b) and the amount of migration slightly increased with the concentration of Zr⁴⁺ increasing. The lattice parameters calculated from interplanar distances²⁶ suggested that the unit cell underwent a shrinkage of a and b and a expansion of c when Zr substituted V in VO₂. At a doping level of 9.8%, the lattice parameters for a and b decreased from 5.748 to 5.745 Å and from 4.532 to 4.526 Å, respectively; meanwhile, that for c increased from 5.353 to 5.360 Å, representing a 0.3% expansion in volume.

X-ray photoelectron spectroscopy (XPS) of as-obtained Zr-doped VO₂ nanoparticles were described as Figure 1c and 1d. The binding energy of the V2p_{3/2} peaks centered at 516.5 eV (Figure 1c) was in good agreement with 515.8 eV of pure VO₂.³⁹ The difference in the binding energy between O1s and V2p_{3/2} was 14.0 eV, corresponding to that value of literature (14.2 eV).⁵ Combined with the results of XRD, the data of XPS provided the auxiliary evidence of VO₂ (M1). Figure 1d showed the binding energies of Zr3d_{5/2} and Zr3d_{3/2}, at 182.7 eV and 185.0 eV, respectively. The difference between the energies were consistent with reported data

in ZrO_2 (2.4 eV),⁴⁰ revealing the existence of Zr^{4+} and identical valence state of Zr and V elements in VO_2 .

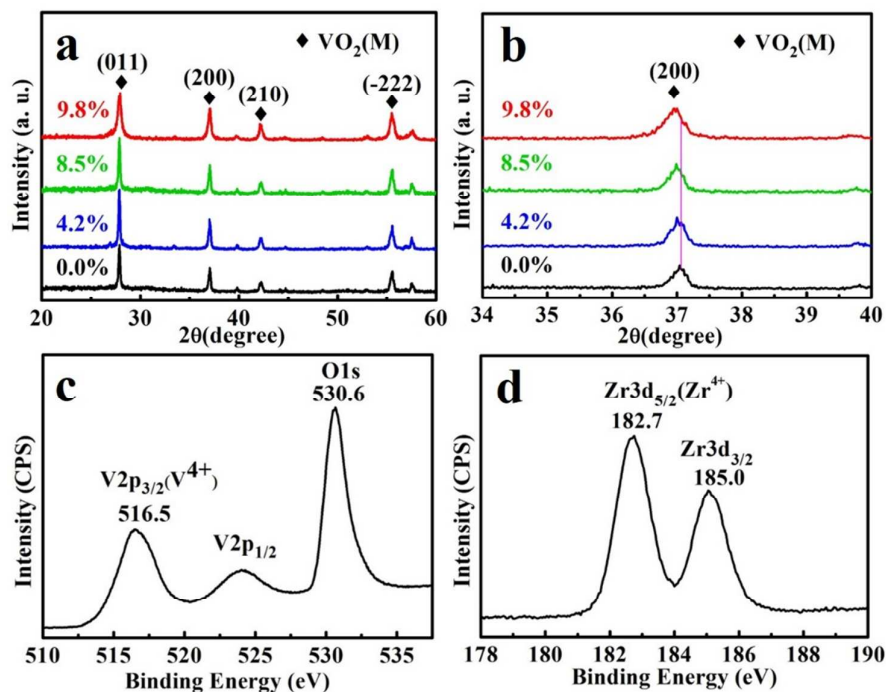


Figure 1 (a) XRD patterns of the pristine and Zr-doped VO_2 nanoparticles and magnifications of the (200) peaks (b). Core level spectra of V 2p (c) and Zr 3d (d) for 4.2 % Zr-doped VO_2 .

The morphology of the Zr-doped VO_2 nanoparticles (4.2 % doping) were studied by TEM (Figure 2a), which showed the spherical appearance of VO_2 nanoparticles and that the diameter sizes of VO_2 nanoparticles ranged from 20nm to 50nm. Selected area electron diffraction (SAED) patterns (the inset in Figure 2a) and the high-resolution TEM (HRTEM) images (Figure 2b) revealed that the VO_2 nanoparticles possessed high crystallinity and could be indexed to VO_2 (M1), which were consistent with the XRD patterns. Moreover, the EDS results in Figure 2c verified the doping of Zr into the nanoparticles.

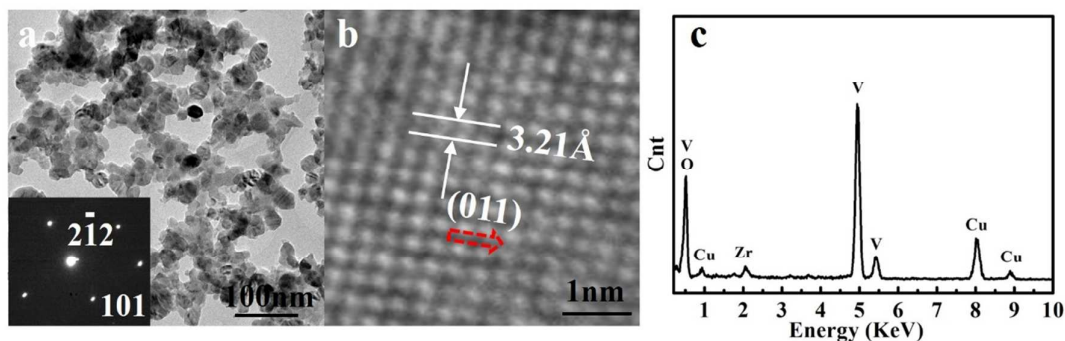


Figure 2 TEM, HRTEM, SAED patterns and EDS results of 4.2% Zr-doped VO₂. (a) TEM (inset, SAED pattern). (b) HRTEM. (c) EDS results.

The metal-semiconductor transition

The phase transition temperature (T_c) of Zr-doped VO₂ nanoparticles was characterized via differential scanning calorimetry (DSC) as shown in Figure 3a. The undoped VO₂ exhibited the T_c of 68.6 °C, which was consistent with previously reported values.^{41,42} The T_c slightly decreased with Zr doping, reaching 64.3 °C at 9.8 at. % Zr doping. This phenomenon may be related to changes in the crystalline structure and difference in electronegativity between Zr (1.33) and V (1.63). The latent heat of the metal-semiconductor transition (MST) (Figure 3b) increased from 27.59 to 31.69 J·g⁻¹ at 4.2 % doping, but it decreased to 30.96 J·g⁻¹ at 8.5 % doping and further declined to 28.01 J·g⁻¹ at 9.8 % doping. Even so, the value at 9.8 % doping was still higher than that of undoped VO₂.

The crystallinity reflects the heat of MST in undoped VO₂ system, and our previous work has described that the doping-induced retardation should be taken consideration as well as the crystallinity to explain the change of latent heat in doping systems²⁶. At low doping level, 4.2 % Zr caused little retardation of the phase transition, exhibiting a higher value of latent heat. As Zr content increased, the retardation played the dominant role and led to a reduction in the latent heat. Since the latent heat of MST reflected the capability of VO₂ nanoparticles undergoing the phase transition, it could also correspond to the value of ΔT_{sol} of the VO₂-nanoparticle-derived foils, thus suggested the change trend of ΔT_{sol} (Figure 4b).

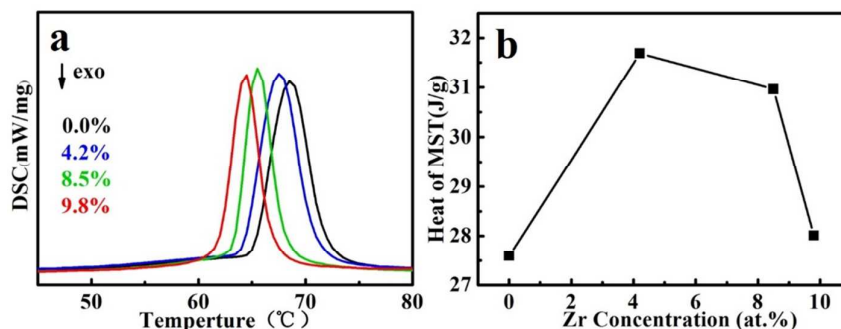


Figure 3 (a) DSC heat flow of the VO₂ nanoparticles doped with different quantities of Zr⁴⁺ (at. %); (b) the experimental latent heat of the MST.

The thermochromic characteristics of Zr-doped VO₂ foils

The UV-Vis-NIR transmittance spectra (Figure 4a) of the Zr-doped VO₂ foils were obtained at 25 °C and 90 °C, respectively. As shown in Figure 4b, the luminous transmittance (T_{lum}) at 25 °C increased from 49.4 % to 60.4 % at 9.8 % doping, while the solar energy modulation ability (ΔT_{sol}) reached a maximum value of 15.3 % at 4.2 % doping and subsequently decreased to 14.1 % at 9.8 % doping, still superior to that value of the undoped VO₂ foil (11.9 %). The variation of ΔT_{sol} was consistent with the change trend of the transition heat (Figure 3b). It was obvious that Zr doping at finite levels could simultaneously enhance the T_{lum} and ΔT_{sol} of VO₂ foils. Our Zr-doped VO₂ foils exhibited better performance compared with a single-layered VO₂ film (T_{lum} =41 %, ΔT_{sol} =6.7 %),⁸ a TiO₂-VO₂ double-layered film (T_{lum} =58 %, ΔT_{sol} =10.9 %),¹⁸ VO₂-ATO-polymer composite foil (T_{lum} =53 %, ΔT_{sol} =11.7 %)³² and Mg-doped VO₂ film (T_{lum} =51 %, ΔT_{sol} =4.0 %)²⁸. Our results were comparable to that of the Ti-doped VO₂ foil with T_{lum} and ΔT_{sol} at 53 % and 17.2 %, ²⁶ respectively, and demonstrated improvements in the Mg-doped VO₂ foils with T_{lum} at 54.2 % and ΔT_{sol} at 10.6 %.²⁵ Despite the better performance of the T_{lum} and ΔT_{sol} , T_c was still much higher than the room temperature (20 °C⁹) and needed to be further modulated.

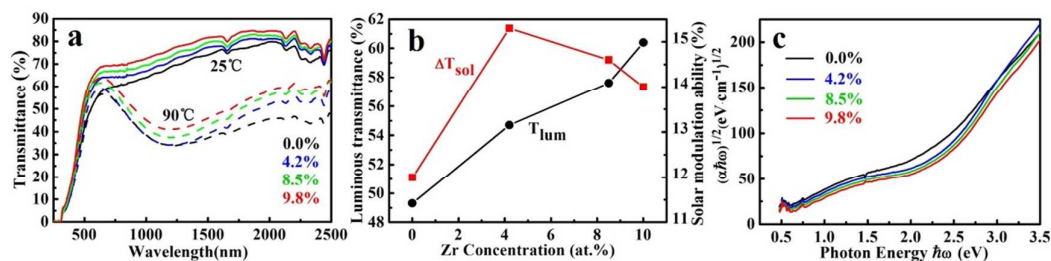


Figure 4 The optical properties of a pure VO₂ and Zr-doped VO₂ foils with various Zr doping contents. (a) The transmittance spectra at 25 °C and 90 °C. (b) The luminous transmittance and solar energy modulation ability. (c) The relationship between $(\alpha\hbar\omega)^{1/2}$ and $\hbar\omega$ for the VO₂ foils doped with varying quantities of Zr (at. %).

To further explain the effect of Zr doping on the optical properties of VO₂ foils, the $(\alpha\hbar\omega)^{1/2}$ vs phonon energy ($\hbar\omega$) for Zr-doped VO₂ foils with different Zr contents were provided in Figure 4c, and the experimental optical band gap (denoted as E_g) was determined by linear extrapolation of $(\alpha\hbar\omega)^m$ vs $\hbar\omega$ near the band gap.²⁵ It was shown that Zr doping widened the optical gaps of the VO₂ foils along with increasing doping levels, from 1.59 eV to 1.89 eV (Figure 4c), exhibiting the same trend with the reference.¹⁰ The obvious improving of E_g to higher energy resulted in a significant decrease in the luminous absorbance, leading to distinctly enhanced luminous transmittance and color change.

The DFT-based first-principles calculations were also performed to unravel tailoring mechanism of dopant Zr on the optical properties in the VO₂ foils. We firstly relaxed Zr-doped VO₂ structures, ZrV₁₅O₃₂ and ZrV₇O₁₆, which were corresponding to doping level of 6.3% and 12.5%. Zr-substitution for V led to the local lattice distortion due to the difference of their ionic radius. Based on the relaxed structures, we further calculated total densities of states (DOSs) of VO₂, ZrV₁₅O₃₂ and ZrV₇O₁₆ to elucidate electron redistribution due to Zr doping. As shown in Figure 5, the calculated intrinsic and optical band gap for pure VO₂ (M) was 0.59 eV and 1.82 eV, respectively, consistent with reported experimental and simulated values.^{10,24} More importantly, we found that the calculated optical band gap increased from 1.82 eV in pure VO₂ to 1.86 eV in ZrV₁₅O₃₂, and 1.93 eV in ZrV₇O₁₆, which was consistent with the experiment (Figure 4c) and led to the enhancement of T_{lum} .

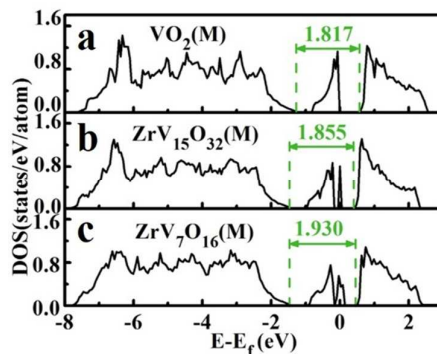


Figure 5 Theoretical calculations. The total density of states for (a) VO_2 (M), (b) $\text{ZrV}_{15}\text{O}_{32}$ (M), (c) $\text{ZrV}_7\text{O}_{16}$ (M).

Color of the Zr-doped and W-Zr-codoped VO_2 foils

The colors of Zr-doped and W-Zr-codoped VO_2 composite foils were characterized by chrominance^{25, 27}. More detailed information about the prepared composite foils such as the morphologies of surface and cross section have been discussed in our recent study.²¹ Figure 6 and Table 1 showed that Zr doping resulted in the yellowish color lightening and brightness improving. This color change originated from the band gap widening of Zr doping. The color of W-Zr-codoped VO_2 foils was slightly weakened compared with undoped foils. From previous Mg and F doping works, we have already known that the aim of color modulation is to adjust a^* and b^* values from positive to approximately zero, however, the color fading due to Zr doping or W-Zr-codoping could not achieve the aim of colorless foils.

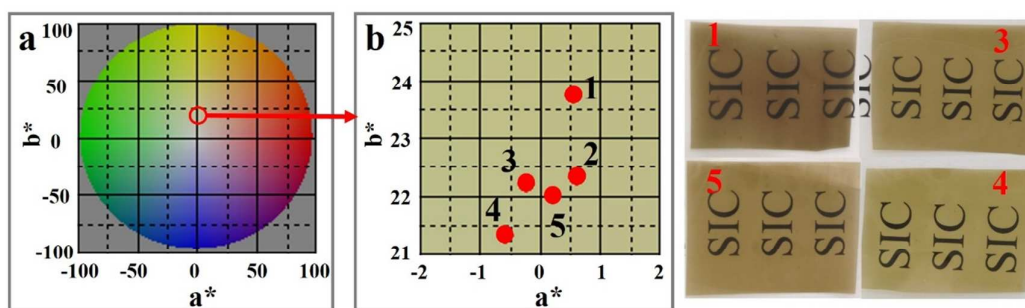


Figure 6 The color of the Zr-doped and W-Zr-codoped VO_2 foils depicted in the spectra magic and graphs of foils.

Table 1. CIE parameters of the Zr-doped and W-Zr-codoped VO_2 foils.

W contents (at. %)	Zr contents (at. %)	L^*	a^*	b^*
0.0	0.0 (1)	60.38	0.54	23.72
0.0	4.2 (2)	60.29	0.62	22.31
0.0	8.5 (3)	63.22	-0.22	22.19
0.0	9.8 (4)	65.56	-0.59	21.31
1.3	8.5 (5)	61.42	0.31	22.07

From aforementioned discussion, one can conclude that Zr doping can decrease the T_c , increase the T_{lum} , improve the ΔT_{sol} and lighten the yellowish color simultaneously. As shown in Table 2, different influences on the properties of Zr doping and previous studies were summarized. Previous works on V-Zr-O system have found that ZrO_2/VO_2 films³¹ exhibited higher T_{lum} due to the anti-reflection effect and $VO_2-ZrV_2O_7$ composite film³⁰ showed significantly enhanced luminous transmittances (from 32.3% at Zr/V=0 to 53.4% at Zr/V=0.12) with increasing Zr/V ratios as a result of absorption-edge changes, but both couldn't achieve a better ΔT_{sol} . Multi-layered VO_2 films ($TiO_2/VO_2/TiO_2/VO_2/TiO_2$)²⁰ can significantly improve the ΔT_{sol} (from 6.7 % to 12.1 %) but make little changes on the T_{lum} and T_c . SiO_2/VO_2 core/shell composite foil exhibited acceptable T_{lum} (55.3 %) while the ΔT_{sol} (7.5 %) was still too low and T_c (55.7 °C) was much higher.³³ Subsequent studies of Mg, F, Ti doping²⁵⁻²⁷ provided more options for different needs of parameter regulation, but the excellent balanced performance remained a challenge for these dopants. Recent works of preparing nanoporous films²³ and improving the crystallinity of VO_2 nanoparticles²¹ made progress on the optical properties (T_{lum} =50 %, ΔT_{sol} =14.7 %) or ΔT_{sol} (22.3 %), yet could not take the T_c into account. Besides, the color was reported to be modulated by Mg and F doping.

Table 2. The comparison between this work and previously reported studies on the T_{lum} , ΔT_{sol} , T_c of VO₂ films or foils.

System	T_{lum} (%)	ΔT_{sol} (%)	T_c (°C)
Single-layered VO ₂ film ⁸	41	6.7	60
ZrO ₂ /VO ₂ ³¹	50.5	~8	52
TiO ₂ /VO ₂ /TiO ₂ /VO ₂ /TiO ₂ ²⁰	45	12.1	60
VO ₂ -ZrV ₂ O ₇ composite film ³⁰	53.4	4.8	62.5
SiO ₂ /VO ₂ core/shell composite foil ³³	55.3	7.5	55.7
Mg-doped VO ₂ foil ²⁵	54.2	10.6	60.4
F-doped VO ₂ foil ²⁷	48.7	10.7	35
Ti-doped VO ₂ foil ²⁶	53	17.2	66.9
Nanoporous VO ₂ films ²³	50	14.7	--
Fine crystalline VO ₂ nanoparticles-based foils ²¹	45.6	22.3	78.9
Zr doped VO ₂ foil (this work)	60.4	14.0	64.3

W-Zr codoping for further decreased temperature

To further decrease the transition temperature, W-Zr-codoped VO₂ nanoparticles have been prepared. The X-ray diffraction (XRD) patterns (Figure 7a and b) suggested that W-Zr-codoped VO₂ nanoparticles could be indexed to monoclinic VO₂ (M1) phase. The TEM graphs (Figure 7c) revealed the morphology of W-Zr-codoped VO₂ nanoparticles and the EDS results (Figure 7d) showed the existence of W and Zr elements in the nanoparticles.

The phase transition temperatures (T_c), luminous transmittances (T_{lum}) and solar energy modulation abilities (ΔT_{sol}) of W-Zr-codoped VO₂ foils at optimized concentration were characterized as shown in Table 3. Compared with 8.5% Zr doping, W-Zr codoping decreased T_c from 65.2 °C to 45.3 °C at 1.3 % W content, and meanwhile maintained a high T_{lum} and ΔT_{sol} (57.9 %, 10.2 %). With W concentration reaching up to 2.4 %, the T_c further declined to 28.6 °C, approaching the room temperature (20 °C, ⁹), the T_{lum} decreased to 48.6 % while the ΔT_{sol} was reduced to

4.9 %. It could be found that W and Zr worked together on decreasing the T_c , and the induction of W doping was more important on the reduction, probably because the similar structure of WO_6 with VO_6 octahedra in VO_2 (R) drove the detwisting of the asymmetric monoclinic VO_2 lattice near W cores to form rutile-like VO_2 nuclei and lower the thermal energy barrier for phase transition^{43,44}. The deterioration of the T_{lum} and ΔT_{sol} with W concentration increasing may be caused by the distortion in the VO_2 crystalline lattice due to W atoms^{21,27}, which became more important than the stabilization of Zr doping on the VO_2 structure.

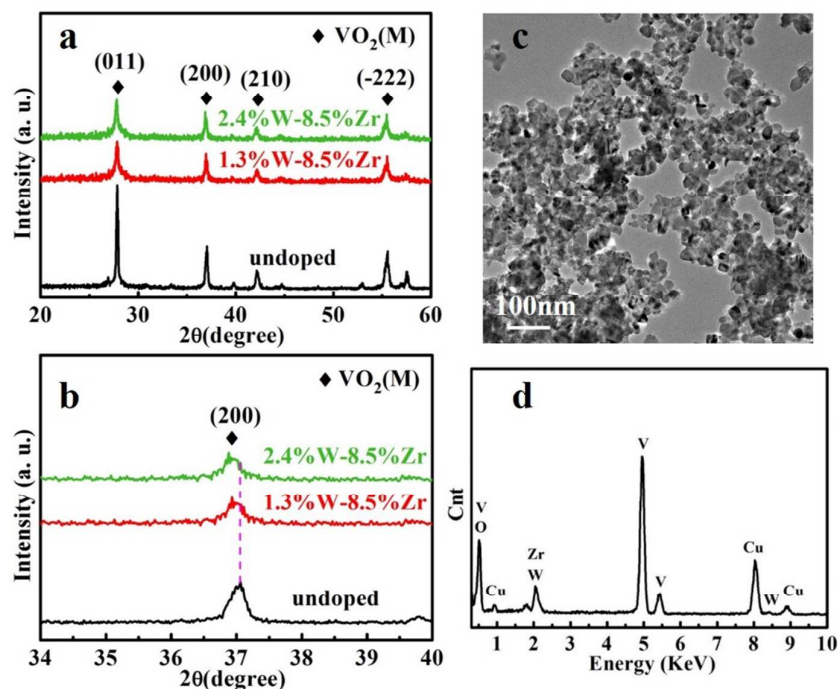


Figure 7 (a) XRD patterns of the pristine and W-Zr-codoped VO_2 nanoparticles, (b) magnifications of the (200) peaks, (c) TEM and (d) EDS results of (1.3 %-8.5 %) W-Zr-codoped VO_2 nanoparticles.

Table 3 The properties of W-Zr-codoped VO_2 foils

W content in VO_2 (at. %)	Zr content in VO_2 (at. %)	T_{lum} (%)		T_{sol} (%)		ΔT_{sol} (%)	T_c (°C)
		25 °C	90 °C	25 °C	90 °C		
0.0	8.5	57.6	52.5	62.2	47.6	14.6	65.2
0.6	8.5	58.4	54.3	61.5	49.2	12.3	55.9
1.3	8.5	57.9	54.6	60.3	50.1	10.2	45.3

1.6	8.5	55.9	54.2	56.7	49.8	6.9	38.7
2.4	8.5	48.6	46.5	50.6	45.7	4.9	28.6

Conclusions

Zr-doped VO₂ nanoparticles and derived flexible solar energy modulation foils were prepared. The XRD and EDS analyses indicated that Zr was successfully doped into the VO₂ lattice. The DSC results demonstrated that Zr doping decreased the T_c (from 68.6 °C to 64.3 °C at 9.8 % doping). The optical properties showed that Zr doping could enhance the luminous transmittance (up to 60.4 %) and improve the solar energy modulation ability (up to 14.1 %). The color change in the VO₂ foils induced by Zr doping was beneficial for applications. The XPS results indicated that Zr⁴⁺ doping maintained the electronic structure stability of VO₂, and the increased latent heat of MST after doping accounted for the improved ΔT_{sol} . First principle calculations gave detailed explanations on the change of transmittance spectra and supported the increase of T_{lum} . The experimental optical band gap of Zr-doped VO₂ nanoparticles exhibited obvious widening, in agreement with the results of calculations. The W-Zr-codoped VO₂ nanoparticles were prepared to further decrease the transition temperature and meanwhile maintain the luminous transmittance and solar energy modulation ability of the derived foils.

Acknowledgements

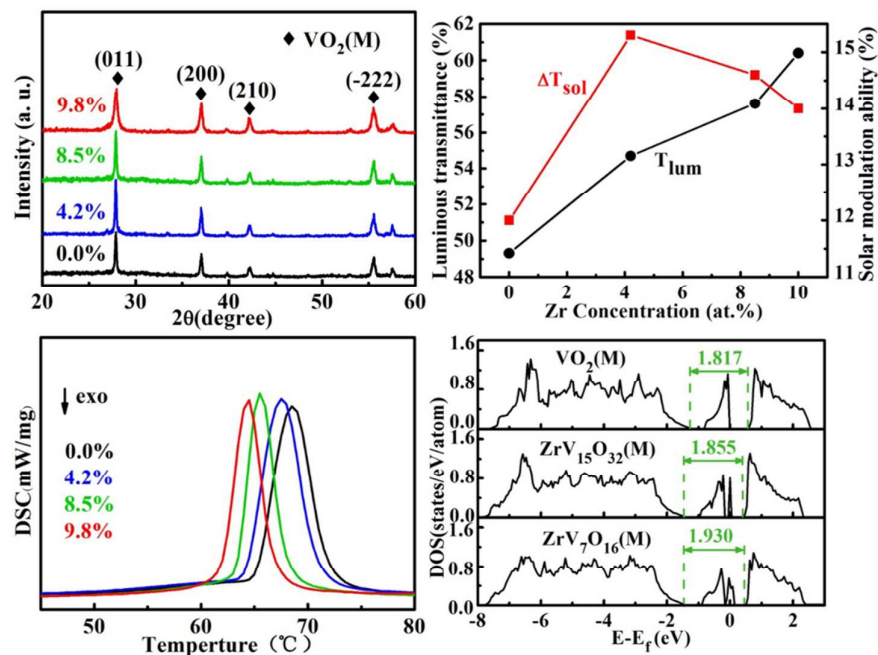
This study was supported in part by funds from MOST (2014AA032802), NSFC (State Outstanding Young Scholars, 51325203) and Innovation Program of Shanghai Municipal Education Commission (14ZZ099).

References

1. R. Binions, G. Hyett, C. Piccirillo and I. P. Parkin, *Journal Of Materials Chemistry*, 2007, **17**, 4652-4660.
2. M. M. Qazilbash, M. Brehm, B.-G. Chae, P. C. Ho, G. O. Andreev, B.-J. Kim, S. J. Yun, A. V. Balatsky, M. B. Maple, F. Keilmann, H.-T. Kim and D. N. Basov, *Science*, 2007, **318**, 1750-1753.
3. Y. W. Lee, B.-J. Kim, J.-W. Lim, S. J. Yun, S. Choi, B.-G. Chae, G. Kim and H.-T. Kim, *Appl Phys Lett*, 2008, **92**, 162903.

4. C. X. Cao, Y. F. Gao and H. J. Luo, *Journal Of Physical Chemistry C*, 2008, **112**, 18810-18814.
5. L. T. Kang, Y. F. Gao and H. J. Luo, *Acs Applied Materials & Interfaces*, 2009, **1**, 2211-2218.
6. L. T. Kang, Y. F. Gao, Z. T. Zhang, J. Du, C. X. Cao, Z. Chen and H. J. Luo, *Journal Of Physical Chemistry C*, 2010, **114**, 1901-1911.
7. S. Y. Li, G. A. Niklasson and C. G. Granqvist, *J Appl Phys*, 2011, **109**, 113515.
8. N. R. Mlyuka, G. A. Niklasson and C. G. Granqvist, *Solar Energy Materials And Solar Cells*, 2009, **93**, 1685-1687.
9. M. Saeli, C. Piccirillo, I. P. Parkin, R. Binions and I. Ridley, *Energ Buildings*, 2010, **42**, 1666-1673.
10. S. Y. Li, G. A. Niklasson and C. G. Granqvist, *Thin Solid Films*, 2012, **520**, 3823-3828.
11. A. Romanyuk, R. Steiner, L. Marot and P. Oelhafen, *Solar Energy Materials And Solar Cells*, 2007, **91**, 1831-1835.
12. L. Whittaker, T.-L. Wu, C. J. Patridge, G. Sambandamurthy and S. Banerjee, *Journal Of Materials Chemistry*, 2011, **21**, 5580-5592.
13. Y. Xu, W. Huang, Q. Shi, Y. Zhang, L. Song, Y. Zhang, *J Sol-Gel Sci Techn*, 2012, **64**, 493.
14. Y. F. Zhang, J. C. Zhang, X. Z. Zhang, C. Huang, Y. L. Zhong and Y. Deng, *Mater Lett*, 2013, **92**, 61-64.
15. Y. Muraoka and Z. Hiroi, *Appl Phys Lett*, 2002, **80**, 583.
16. L. Dai, C. X. Cao, Y. F. Gao and H. J. Luo, *Solar Energy Materials And Solar Cells*, 2011, **95**, 712-715.
17. Griffith.Ch and H. K. Eastwood, *J Appl Phys*, 1974, **45**, 2201-2206.
18. Z. Chen, Y. Gao, L. Kang, J. Du, Z. Zhang, H. Luo, H. Miao and G. Tan, *Solar Energy Materials and Solar Cells*, 2011, **95**, 2677-2684.
19. P. Jin, M. Tazawa, K. Yoshimura, K. Igarashi, S. Tanemura, K. Macak and U. Helmersson, *Thin Solid Films*, 2000, **375**, 128-131.
20. N. R. Mlyuka, G. A. Niklasson and C. G. Granqvist, *Phys Status Solidi A*, 2009, **206**, 2155-2160.
21. Z. Chen, Y. Gao, L. Kang, C. Cao, S. Chen and H. Luo, *J Mater Chem A*, 2014, **2**, 2718.
22. L. T. Kang, Y. F. Gao, H. J. Luo, Z. Chen, J. Du and Z. T. Zhang, *Acs Applied Materials & Interfaces*, 2011, **3**, 135-138.
23. X. Cao, N. Wang, J. Y. Law, S. C. Loo, S. Magdassi and Y. Long, *Langmuir*, 2014, **30**, 1710-1715.
24. S. L. Hu, S. Y. Li, R. Ahuja, C. G. Granqvist, K. Hermansson, G. A. Niklasson and R. H. Scheicher, *Appl Phys Lett*, 2012, **101**, 201902
25. J. D. Zhou, Y. F. Gao, X. L. Liu, Z. Chen, L. Dai, C. X. Cao, H. J. Luo, M. Kanahira, C. Sun and L. M. Yan, *Phys Chem Chem Phys*, 2013, **15**, 7505-7511.
26. S. Chen, L. Dai, J. Liu, Y. Gao, X. Liu, Z. Chen, J. Zhou, C. Cao, P. Han, H. Luo and M. Kanahira, *Phys Chem Chem Phys*, 2013, **15**, 17537-17543.
27. L. Dai, S. Chen, J. Liu, Y. Gao, J. Zhou, Z. Chen, C. Cao, H. Luo and M. Kanahira, *Phys Chem Chem Phys*, 2013, **15**, 11723-11729.
28. N. R. Mlyuka, G. A. Niklasson and C. G. Granqvist, *Appl Phys Lett*, 2009, **95**, 171909.
29. L. Zhao, Z. Wu, Y. Jiang, *The experimental science and technology*, 2006, **4**, 113. (in Chinese)
30. J. Du, Y. Gao, H. Luo, Z. Zhang, L. Kang and Z. Chen, *Solar Energy Materials and Solar Cells*, 2011, **95**, 1604-1609.
31. G. Xu, P. Jin, M. Tazawa and K. Yoshimura, *Solar Energy Materials and Solar Cells*, 2004, **83**, 29-37.

32. Y. Gao, S. Wang, H. Luo, L. Dai, C. Cao, Y. Liu, Z. Chen and M. Kanehira, *Energ Environ Sci*, 2012, **5**, 6104.
33. Y. Gao, S. Wang, L. Kang, Z. Chen, J. Du, X. Liu, H. Luo and M. Kanehira, *Energ Environ Sci*, 2012, **5**, 8234.
34. S. Y. Li, G. A. Niklasson and C. G. Granqvist, *J Appl Phys*, 2010, **108**, 063525.
35. G. Kresse and J. Furthmuller, *Phys. Rev. B*, 1996, **54**, 11169-11186.
36. G. Kresse and D. Joubert, *Phys. Rev. B*, 1999, **59**, 1758-1775.
37. W. E. Pickett, S. C. Erwin and E. C. Ethridge, *Phys. Rev. B*, 1998, **58**, 1201-1209.
38. R. J. O. Mossaneck and M. Abbate, *Phys. Rev. B*, 2006, **74**, 125112.
39. G. Silversmit, D. Depla, H. Poelman, G. B. Marin and R. De Gryse, *Journal of Electron Spectroscopy and Related Phenomena*, 2004, **135**, 167-175.
40. S. J. Wang and C. K. Ong, *Appl Phys Lett*, 2002, **80**, 2541.
41. M. Netsianda, P. E. Ngoepe, C. Richard, A. Catlow and S. M. Woodley, *Chemistry Of Materials*, 2008, **20**, 1764-1772.
42. C. Wu, X. Zhang, J. Dai, J. Yang, Z. Wu, S. Wei and Y. Xie, *Journal of Materials Chemistry*, 2011, **21**, 4509.
43. X. Tan, T. Yao, R. Long, Z. Sun, Y. Feng, H. Cheng, X. Yuan, W. Zhang, Q. Liu, C. Wu, Y. Xie and S. Wei, *Sci Rep-Uk*, 2012, **2**, 466.
44. J. Zhang, H. He, Y. Xie and B. Pan, *J Chem Phys*, 2013, **138**, 114705.



The effect of Zr doping on the T_c , T_{lum} and ΔT_{sol} of VO₂